Nuclear Inst. and Methods in Physics Research, A 903 (2018) 140–146

Contents lists available at ScienceDirect

Nuclear Inst. and Methods in Physics Research, A

journal homepage: www.elsevier.com/locate/nima

A low-power laserwire profile monitor for H⁻ beams: Design and experimental results

T. Hofmann [a,b,*], G.E. Boorman [a], A. Bosco [a], S.M. Gibson [a], F. Roncarolo [b]

[a] John Adams Institute at Royal Holloway, University of London, Egham, TW200 EX, United Kingdom
[b] Beam Instrumentation Group, CERN, CH-1211 Geneva 23, Switzerland

ARTICLE INFO

Keywords:
Laserwire
Linac
Profile
H⁻
Diamond
Fibre optics

ABSTRACT

An instrument to non-destructively measure the transverse profile of an H⁻ beam has been developed and tested at CERN's new LINAC4. The vertical profile of the H⁻ beam has been measured, at beam commissioning energies of 50, 80 and 107 MeV. The instrument consists of a laser-source which is coupled to an optical fibre, delivering laser pulses with hundreds Watts of peak power to the accelerator tunnel, where the laser beam is focused horizontally onto the H⁻ beam. Due to photo-detachment, electrons are liberated from the ions and can be deflected by a weak dipole field onto a diamond detector. The beam profile is obtained by scanning the laser beam vertically across the H⁻ beam and recording for each position the number of arriving electrons. The design, implementation and characterisation of the novel instrument shall be described and the measured beam profiles compared to profiles obtained with SEM-grids and wirescanners.

1. Introduction

To measure beam profiles at ion beam accelerators, interceptive methods such as wirescanners or secondary electron emission (SEM) grids are used predominantly [1]. These techniques have been used for decades and offer with a simple design reliable profile measurements. Crossing the particle beam with a solid wire however, causes challenges due to heating such that a certain risk of breakage and subsequent vacuum contamination cannot be avoided. In addition, the induced scattering on the beam causes losses and emittance blow-up, so that the instrument degrades the beam quality.

Due to these arguments non-destructive profile monitors, which cross the ion beam with a laser beam instead of a solid wire are increasingly prevalent. The principle of the laserwire is similar to a wirescanner but without the risk of vacuum contamination and noticeable effect on the ion beam and it can be used over a wide range of beam energies (MeV...Multi-GeV). An example of a sophisticated laser-based system can be found at the Spallation Neutron Source at Oak Ridge, Tennessee [2]. In this system a free-space laser beam with MW peak power is split up to supply 9 interaction stations with the H⁻ beam where the detached electrons are collected by Faraday cups.

The setup which is presented in this paper is based on the basic principle as shown in Fig. 1. The low-power laser beam is delivered by an optical fibre and the electrons are sensed with a high sensitive diamond detector, such that the instruments precision and reliability is enhanced.

The laser beam is focused to a waist size approximately 10 times smaller than the H⁻ beam at the interaction point. Due to the photo-detachment mechanism,

$$H^- + \gamma \rightarrow H^0 + e^- \tag{1}$$

electrons can be stripped from the H⁻ ions. The probability for each ion crossing the laser beam to be stripped is

$$\mathbb{P}_{PD} = 1 - e^{-\sigma_{PD}(\lambda'_L)\cdot F_L \cdot t} \tag{2}$$

where σ_{PD} is the cross-section [3] at a laser wavelength λ_L, F_L the photon flux and t the time of flight of the particle across the laser beam [4]. The process cross-section σ_{PD} is influenced by the relativistic Doppler shift as described in [5]. Minor changes have been summarised in Table 1, together with the laser wavelength λ'_L in the rest-frame of the H⁻ beam for the relevant beam energies.

The small portion of liberated electrons are deflected by a weak dipole field towards an integrating detector while the main H⁻ beam experiences just a minor deflection (mrad). Scanning the laser beam vertically across the H⁻ beam, the beam profile can be reconstructed from the corresponding number of arriving electrons at the detector.

* Corresponding author at: John Adams Institute at Royal Holloway, University of London, Egham, TW200 EX, United Kingdom.
E-mail address: thomas.hofmann@cern.ch (T. Hofmann).

https://doi.org/10.1016/j.nima.2018.06.035
Received 16 March 2018; Received in revised form 28 May 2018; Accepted 11 June 2018
Available online 21 June 2018

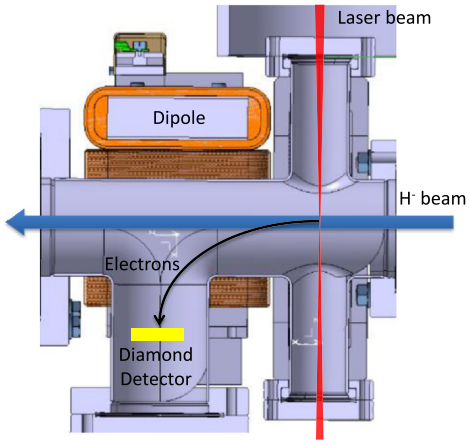

Fig. 1. Top view of the concept for laser-based vertical profile measurements. A laser beam is focused onto the H- beam. The detached electrons are steered by a weak dipole field onto a diamond detector.

Table 1
Change of photo-detachment cross-section due to relativistic Doppler-effect.

E_{kin} [MeV]	λ'_L [nm]	$\sigma_{PD}[10^{-17}\text{cm}^2]$
0	1064	3.68
50	1010	3.86
80	980	3.94
107	957	3.98

Table 2
Characteristics of laser-source.

Parameter	Permissible values	Operational values
Wavelength	1064 nm	1064 nm
Peak power	max. 40 kW	100 W
Pulse length	1 ns...300 ns	100 ns
Pulse frequency	35 kHz...500 kHz	86 kHz
Linewidth	1 nm...5 nm	1 nm...5 nm
M^2	1.3	$M_y^2 = 1.27$

2. Instrument design and implementation

2.1. System design

The instrument design focused on reducing complexity compared to preceding laserwire instruments and thus creating a reliable device which is nevertheless able to measure the beam characteristics with high precision. The key element of this approach is a comparably low power laser system with fibre-based transmission to the accelerator which is described in the following.

2.1.1. Laser system

To protect the sensitive optical elements in the laser source, a laser room has been built in the klystron gallery above the accelerator tunnel to host the laser source. The laser is configured as Master Oscillator Power Amplifier (MOPA) with a laser diode based optical seed pulse oscillator followed by a dual-stage fibre amplifier system, pumped by multi-mode laser diodes. Key laser parameters are listed in Table 2.

The 75 m long transport line of the laser beam to the beampipe was accomplished with a Large Mode Area (LMA) optical fibre [6], equipped with 330 μm long end-caps to avoid damage induced by the high power densities occurring at the fibre end-facets. The transmission has been characterised for laser pulses with peak power up to 2.2 kW and was found to be above 73% (including fibre coupling losses), slightly decreasing towards higher laser powers [7].

The optics setup situated after fibre transmission to the accelerator tunnel (the laser injector in Fig. 8) is shown schematically in Fig. 2.

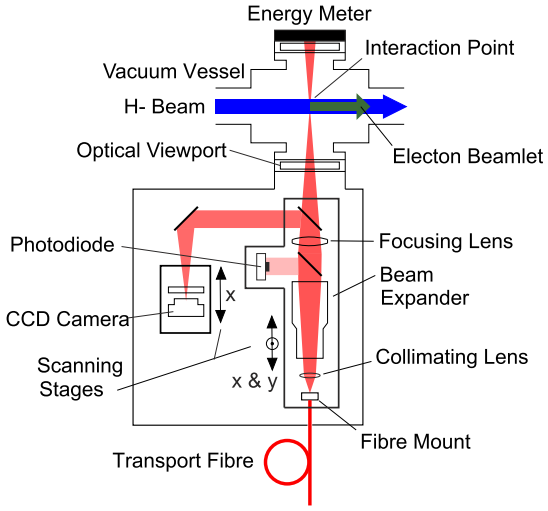

Fig. 2. Top view of optics setup for laser injection into the beampipe and characterisation of the laser beam.

The laser beam exits the transport fibre and is subsequently collimated and enlarged to a 2σ beam radius of approx. 3.8 mm. The expanded laser beam is sampled via an optical flat window, AR-coated on only one side, which creates a weak Fresnel reflection directed towards the photodiode for online monitoring of the laser pulse-shape. After passing a lens ($f = 600$ mm), the laser beam enters the vacuum chamber, interacts at its waist with the H^- beam and exits the vacuum chamber. Hereafter it is absorbed by an integrating energy metre to monitor online the laser pulse energy for an absolute calibration.

To perform a vertical scan of the laser beam via the H^- beam, the fibre coupled beam delivery optics is mounted on a remote controlled stage. An additional stage in the horizontal plane is used to position the laser waist precisely at the centre of the beampipe. In normal operation, the laser beam enters the vacuum chamber through the viewport, however, when the stage is at its lowest position, the beam is deflected to enable self-diagnostics. With a CCD camera mounted on a horizontal stage, the transverse shape of the laser-waist can be characterised and the beam quality (M^2) of the laser beam can be determined.

2.1.2. Electron deflection

To achieve a simple and cost-effective solution for deflecting the electrons, it was decided to modify a LINAC4 type steerer magnet. By removing the magnet coil on the T-chamber side, the steerer acts as a C-shaped magnet with the remaining coil powered to create the B-field (see Fig. 1). A photograph of the full setup installed at the diagnostic testbench at LINAC4 can be seen in Fig. 3.

The trajectory of the electrons in the magnetic field were simulated to ensure that they do not collide with the vacuum chamber wall and furthermore to determine the spot size of the electrons in the plane of the diamond detector.

The following assumes that the field strength scales linear with the coil current thus the simulation will be described just for the 50 MeV H^- beam scenario. In this case the kinetic energy of each electron is 27 keV, as can be derived from the 50 MeV kinetic energy of the H^- ions and the proton to electron mass ratio. These low energy electrons can be deflected by 90° with an integrated field of 0.9 mTm.

A magnetic field-map was created to predict the electron trajectories in the B-field, which can be seen in Fig. 4. Starting from LINAC4 beam dynamics simulation of the H^- distribution in the plane of the laser interaction ($x = 0$ mm; $z = -83$ mm), the trajectories of the stripped electrons to the detector plane within the magnetic vector-field were calculated. In addition to the Lorentz force, space-charge effects of the

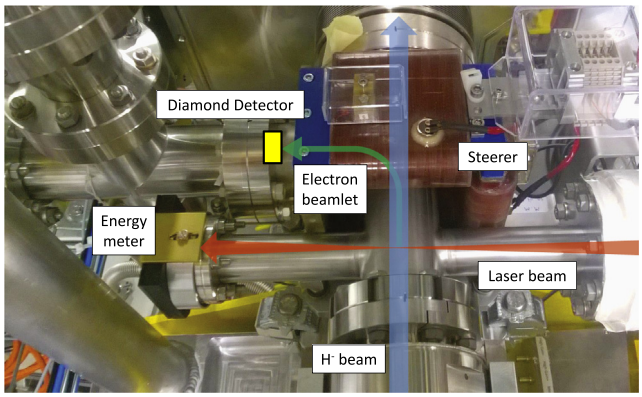

Fig. 3. Photo of vacuum-chamber for laser interaction with associated steerer magnet to deflect electrons towards the diamond detector.

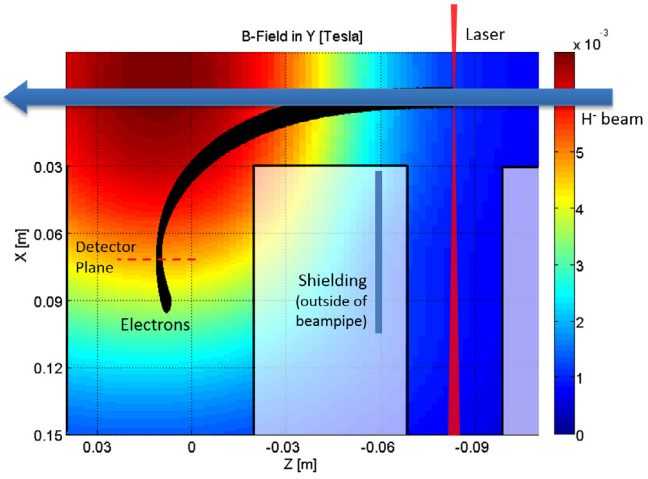

Fig. 4. Magnetic field map (in Tesla) and electron trajectories (black) from the laser interaction point to the diamond detector. White areas are outside of the vacuum chamber.

main H^- beam and synchrotron radiation were taken into account but had no significant effects on the path of the electrons.

The black curve in Fig. 4 represents the $\pm 3\sigma$ envelope of the electron trajectory when powering the magnet coil with a current of 4.7 A. Shielding at $z = -60$ mm surrounds the beampipe between laser interaction point (IP) and steerer magnet. This shielding was designed to shape the magnetic field lines such that the electrons do not strike the wall of the beam pipe before reaching the electron monitor. The detector plane $x = 72$ mm was chosen, as this is the focal point generated by the weak focusing of the dipole. In this plane the simulation of the electron beamlet size for one laser position yielded $\sigma_z = 230 \pm 30$ µm and $\sigma_y = 110 \pm 15$ µm. It has to be mentioned, that the magnetic vector-field of the steerer magnet was not verified by a scan with a Hall-probe due to time constraints. As result a systematic uncertainty of the electron path is present in this simulation.

The effect of the dipole field on the main H^- beam is an angular kick in the horizontal plane of 1.6 mrad, which is insignificant in this setup as the beam is dumped shortly afterwards (see Fig. 8).

2.1.3. Diamond detector

A single crystal (sCVD) diamond detector has been designed, to detect the liberated low-energy electrons ($E_{kin} = 27$ keV for 50 MeV H^- beam). Its 4 mm x 4 mm active surface is sufficient to capture all arriving electrons per laser position when moved in synchronisation

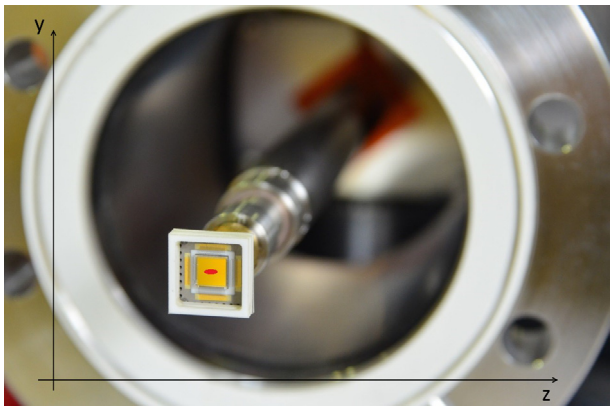

Fig. 5. sCVD diamond detector [8] mounted on a vertical actuator; Dimensions ($\pm 3\sigma$) of an arriving electron beamlet marked as ellipse.

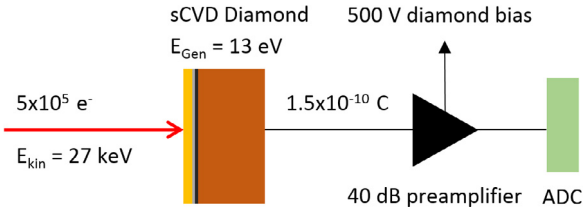

Fig. 6. Signal creation and readout of the diamond detector.

with the laserwire. Due to its small dimensions the low capacitance permits detections of the 100 ns long pulses without low-pass distortion.

Fig. 5 shows the diamond detector mounted in the beampipe on a vertical actuator. The front electrode of the detector is bonded to ground potential all around its perimeter to avoid electro-magnetic disturbance from the main H^- beam passing just 72 mm away from the detector. It consists of 3 thin layers (250 nm gold, 120 nm platinum and 100 nm titanium) which ensure that even for the lowest electron energy (27 keV) just 3.2 keV is lost in the front electrode. The ellipse at the detector surface represents the $\pm 3\sigma$ dimensions of a typical electron beamlet as reference.

In Fig. 6 the signal chain up to the analogue to digital converter (ADC) is illustrated. A laser pulse with 100 µJ energy hitting the H^- beam centrally will detach approx. $N_{e-} = 5 \cdot 10^5$ electrons from the hydrogen ions. This corresponds to a probability of $4 \cdot 10^{-5}$ for an H^- ion to interact with the laser beam. After initial losses in the front electrode, the remaining kinetic energy of each electron is deposited in the diamond material creating a carrier–hole pair for each $E_{Gen} = 13$ eV. The cumulative charge of

$$Q_{cum} = \frac{eN_{e-} \cdot (E_{kin} - E_{loss})}{E_{Gen}} = 1.5 \cdot 10^{-10}\ \mathrm{C} \tag{3}$$

is read out applying a bias voltage of 500 V and is pre-amplified by 40 dB gain. An ADC running at 1 GS/s records the signal for further digital signal processing.

2.2. Experimental setup

The developed instrument has been operated during commissioning of LINAC4, measuring beams of 50 MeV, 80 MeV and 107 MeV kinetic energy. The vertical RMS beam sizes for all commissioning periods were in the range from 1 mm to 2 mm and the H^- beam current between 15 mA and 25 mA depending on the source and accelerator performance. The time structure of the H^- beam is shown in Fig. 7.

The diagnostics bench shown in Fig. 8 was moved downstream as each section of LINAC4 was completed, enabling the emerging beam

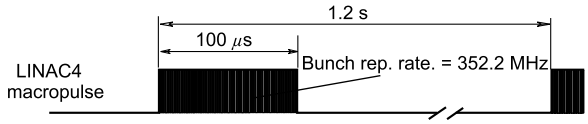

Fig. 7. Time structure of the LINAC4 H⁻ beam.

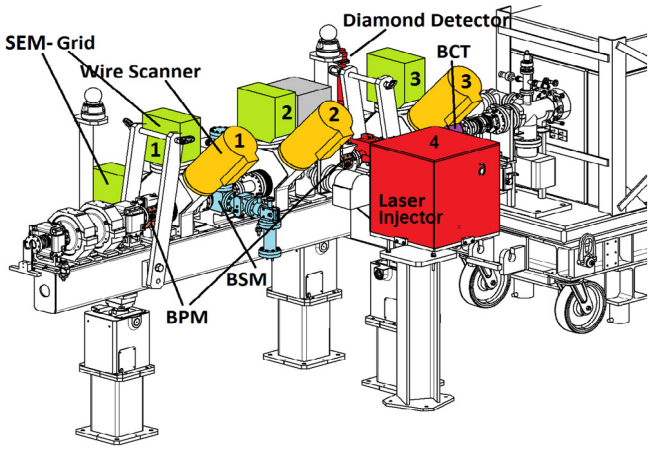

Fig. 8. Diagnostic testbench used for beam commissioning at 50 MeV, 80 MeV and 107 MeV H⁻ beam. [9].

at each commissioning step to be characterised. It consists of several diagnostic instruments, most relevant for this study were the Secondary-Emission (SEM)-grids and wirescanners for transverse beam monitoring in 3 planes. The laser-injector for vertical profile measurements is marked with (4).

3. System characterisation

3.1. Laser beam properties at IP

The resolution of the profile measurement is related directly to the laser beam properties at the IP. Thus an in-situ characterisation of the laser waist has been performed with the setup shown in Fig. 2. The result is plotted in Fig. 9 and shows improved performance regarding previous measurement campaigns [5]. Due to the new laser source a lower M^2 factor could be achieved, which resulted in a 20% increase of the Rayleigh length (x_R/y_R) and a 8% thinner waist ($w_{x/y}$) in both planes. The resolution of the instrument is dependent on the laser diameter but also on its pointing stability. Due to the fibre-based delivery line no relevant instabilities have been observed on the CCD camera (see Fig. 2), thus the instrument resolution is defined by the vertical laser beam waist of $\pm 2\,\sigma = \pm 67$ μm. The observed astigmatism does not perturb the measurement as only the vertical plane is relevant in this application.

At the desired working point ($t_{pulse} = 100$ ns; $E_{pulse} = 10$ μJ; $f_{laser} = 86$ kHz) the pulse-to-pulse power fluctuations of the laser have been measured as they can become a significant error source of the instrument (see Eq. (2)). An RMS pulse energy stability of 3% after propagation through the 75 m fibre has been found. To eliminate this introduced error, the signal of the diamond detector was normalised by the photodiode signal recorded just before the IP (see Fig. 2).

3.2. Diamond raw signal analysis

Fig. 10 shows the signal of the diamond detector recorded on an 80 MeV H⁻ beam with average H⁻ beam current of 14 mA. Each segment corresponds to a time window of 1.5 μs around each laser pulse, recorded at a laser repetition frequency of 86 kHz which is synchronised with a

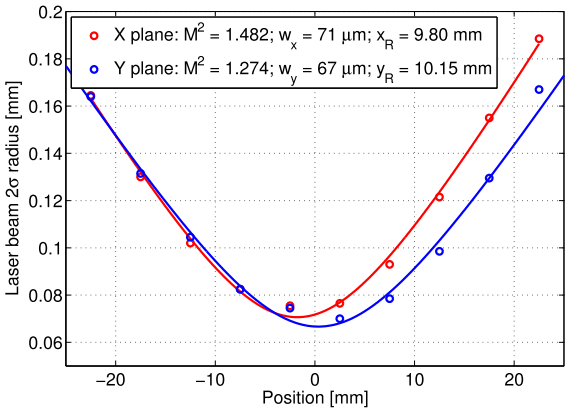

Fig. 9. Spatial properties of laser beam at the IP with H⁻ beam.

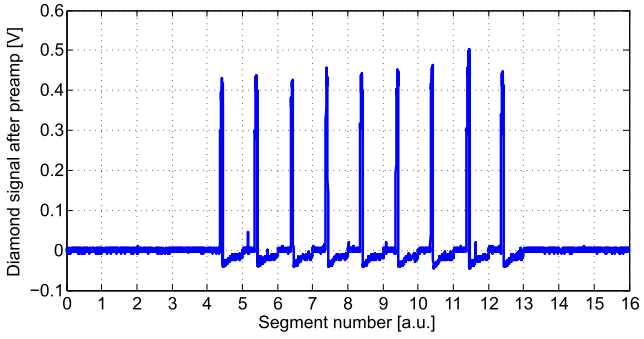

Fig. 10. Diamond signal recorded in segments.

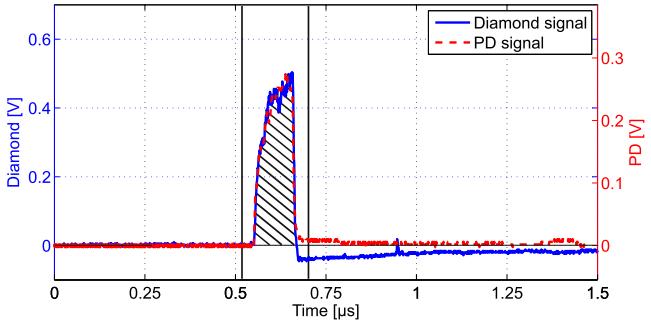

Fig. 11. Single segment of diamond signal compared with photodiode signal of laser pulse.

sub-harmonic of the LINAC4 bunch frequency (352.2 MHz). The 9 pulses are the signals of the liberated electrons, created by the laser pulses which interact with the 100 μs long H⁻ beam pulse.

In Fig. 11 an example segment is plotted. A very clear diamond detector signal with a pulse-shape and -length similar to the laser pulse was observed without any background floor of non-laser-stripped electrons. The occasional spikes (see 0.95 μs in Fig. 11 and segment 5 and 11 in Fig. 10) were attributed to hits of single protons/H⁻ /H⁰, which were lost from the main beam. At certain beam settings this effect was significantly increased such that some disturbance of the laser-stripped electron-pulse was monitored.

In the data analysis of each detector segment, within pre-defined limits (vertical bars), the positive values were integrated (hatched surface) while the negative part, caused by the AC-coupled readout, was neglected. By repeating this procedure for all segments and averaging

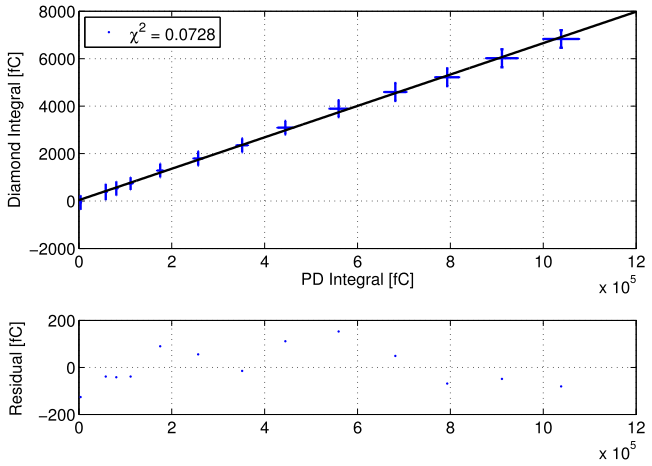

Fig. 12. Integral of pulse recorded with diamond detector versus integral of pulse recoded with the photodiode before the IP with the 50 MeV H- beam (see Fig. 2).

the results, the mean photo-detachment yield during the LINAC4 pulse is gained.

3.3. Diamond linearity

To deduce the linearity of the diamond detector for different electron fluences the laser pulse energy was scanned. For each laser setting the signals on the diamond detector were recorded for 9 H^- beam pulses and the data was analysed as described previously. In Fig. 12 the integrated charge read out from the diamond detector is plotted versus the signal of the photodiode prior to the IP (see Fig. 2). In this way energy-fluctuations of the laser pulse did not perturb the measurement as the corresponding signal from the diamond detector can be assigned pulse to pulse.

The diamond detector signal was found to follow linearly the photodiode signal within error. The small offset of diamond integral was caused by the high proton-background present at this measurement at 50 MeV H^- beam energy.

A similar measurement has been accomplished at 80 MeV beam energy. Although the gradient of the response differs due to the increased kinetic energy of the impinging electrons, the linearity of the detector response is similarly good.

3.4. Electron beamlet size at the diamond detector

The size of the liberated beamlet in the plane of the diamond detector was characterised experimentally to verify the electron tracking simulations [7] and ensure that no laser-stripped electrons miss the active detector surface.

The measurement was accomplished at an 80 MeV H^- beam by scanning the diamond detector vertically with the laser static in the centre of the H^- beam. The horizontal position (z-coordinate) was scanned with the current of the steerer magnet and hereby moved the beamlet position in the z-plane.

The signals arriving at the diamond detector were processed and the integrated charge was plotted in the y-z-plane of the diamond detector as shown in Fig. 13 with the active detector surface (black frame) overlaid as a reference. The invariant signal level in the centre of the detector indicates a beamlet size smaller than the detector dimensions. The beamlet size was determined by calculating the derivative in the y- and z-plane, which resulted in $\sigma_z = 0.4 \pm 0.1$ mm and $\sigma_y = 0.45 \pm 0.1$ mm. Compared to the tracking simulation, the beamlet dimensions are increased by a factor 2 in the z-plane and 4 in the y-plane. We assume that magnetic stray fields, defocusing the electrons are responsible

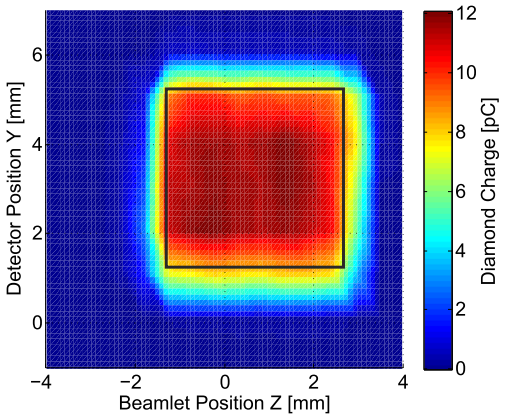

Fig. 13. Signal of diamond detector for different detector positions in Y and different beamlet positions in Z; Black frame as comparison to 4 mm × 4 mm surface of diamond detector.

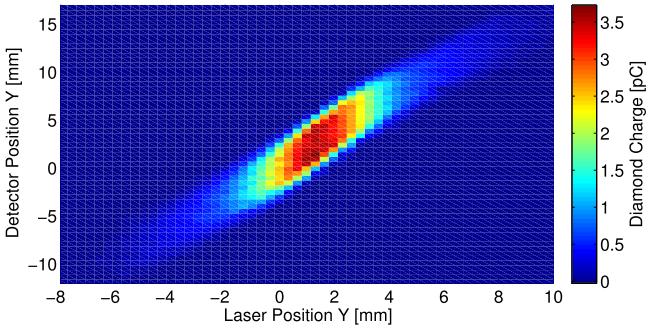

Fig. 14. Diamond signal for different laser and detector positions.

for this discrepancy. Most significantly, the detector surface in both dimensions is clearly sufficiently big to collect all arriving electrons per beamlet.

The measurement of the vertical size of the H^- beam with the laserwire instrument has been performed at 50 MeV, 80 MeV and 107 MeV by a 2-dimensional scan of laser and diamond detector both in the vertical plane, corresponding to the data visualised in Fig. 14. At each laser position the maximum charge value in the range of diamond detector positions was used to plot the beam profile.

To verify the accuracy of the instrument, the recorded beam profiles were compared with SEM-grids and wirescanners installed in the vicinity of the laser (see Fig. 8, only drift spaces between the instruments). In Fig. 15 the measured RMS beam sizes of the 107 MeV beam in different positions along the diagnostic testbench are plotted, with the black line corresponding to an interpolation between the SEM-grid and wirescanner results. The discrepancy from the interpolation and the laser measurements has been found consistently below ±2%.

In Figs. 16–18 the profiles recorded with the laserwire at different beam energies are compared with the profiles from SEM-grids and wirescanners which have been scaled according to the interpolated laser position. The recorded samples of the profile correspond to the mean values over the LINAC4 pulse length and the error bars to the RMS deviation for measurements at multiple LINAC4 pulses. For all beam energies a very close agreement in terms of the RMS-size but also in particular the profile shape can be observed.

4. Summary

We have presented the design of a laserwire profile monitor based on a low-power laser and fibre-optic delivery to the IP with the H^- beam,

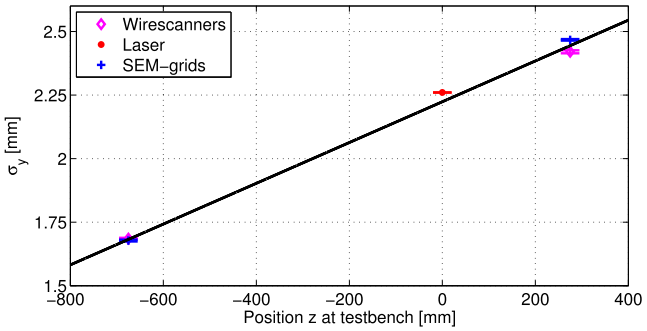

Fig. 15. Beam profile measurements at different positions at the diagnostic testbench.

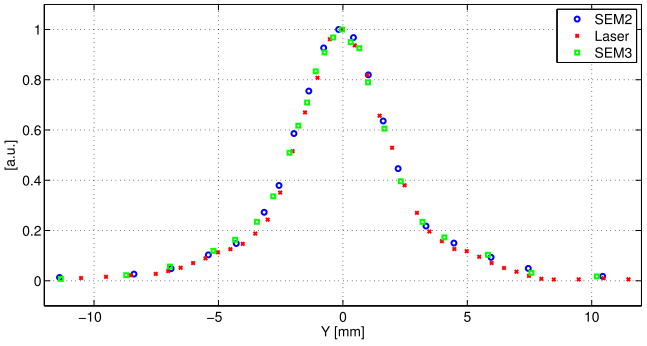

Fig. 16. Overlay of SEM-grid and laserwire profiles, recorded at the 50 MeV beam.

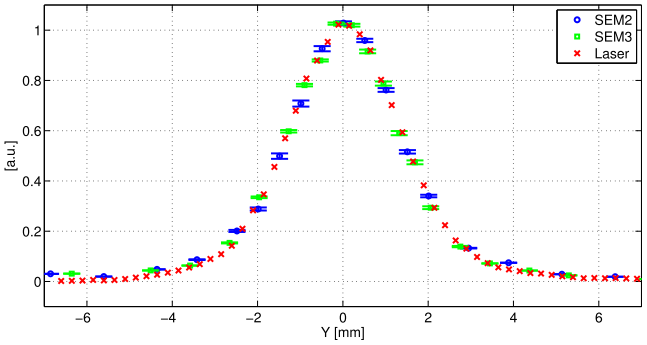

Fig. 17. Overlay of SEM-grid and laserwire profiles, recorded at the 80 MeV beam.

which ensures stable and reliable operation. The subsequent deflection of the laser-detached electrons with a weak dipole field has been simulated and experimentally verified. For sensing the beamlets of low energy electrons an ultra-compact diamond detector has been custom designed.

The performance characteristics of the novel instrument have been systematically verified on the LINAC4 beam. The laser transmission via optical fibre was found to be above 76% in the dedicated working point and the laser beam at the IP exhibited a beam quality factor $M_y^2 < 1.3$, which thus provided an instrument resolution of approx. 70 μm. The response of the diamond detector was analysed for different beam energies and intensities of the laser-detached electron beamlets where a linear behaviour and a high SNR has been found. The size of the

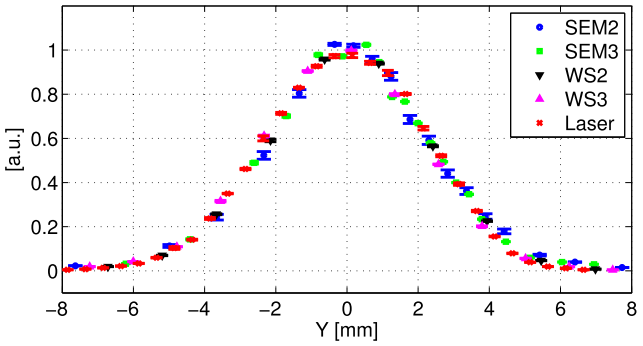

Fig. 18. Overlay of SEM-grid, wirescanner (WS) and laserwire profiles, recorded at the 107 MeV beam.

arriving electron beamlets were measured and found to be consistently smaller than the dimensions of the diamond detector.

Beam profile measurements were conducted at 50, 80 and 107 MeV beam energy and the results were compared with nearby SEM-grids and wirescanners. For all beam energies an outstanding agreement in terms of beam-shape was observed and deviations in terms of the RMS beam size were found below ±2% [10].

The experience and results gained with the presented profile monitor have informed the design of a future laserwire system at LINAC4. Two of these systems have been recently installed in the 160 MeV region [11]. Each instrument is capable of detecting both interaction products, electrons and neutralised H^0 and thus achieve redundant profile and emittance reconstruction [12,13]. Compared with the presented setup, the electron detection method was changed to an electron multiplier which can be mounted at fixed location and is not affected by a potential proton background. In addition, the laser injector was expanded to allow horizontal and vertical injection of the laser beam into the vacuum vessel.

Acknowledgements

We would like to thank our colleagues in the CERN profile measurement section and the LINAC4 operation team for their strong support. Furthermore, we are grateful for fruitful collaborations with CERN's normal conducting magnet group which redesigned the steerer magnet and CIVIDEC GmbH which provided a high-performance diamond detector.

References

[1] M. Plum, Interceptive beam diagnostics - signal creation and materials interactions, in: Proceedings of AIP, vol. 732, Knoxville, Tennessee, 2004, pp. 23–46.
[2] Y. Liu, A. Aleksandrov, S. Assadi, W. Blokland, C. Deibele, W. Grice, C. Long, T. Pelaia, A. Webster, Laser wire beam profile monitor in the Spallation Neutron Source, SNS superconducting linac, Nucl. Instrum. Methods A 612 (2010) 241–253.
[3] J.T. Broad, W.P. Reinhardt, One- and two-electron photoejection from H^-: A multichannel J-matrix calculation, Phys. Rev. A 14 (6) (1976) 2159–2173.
[4] R.C. Connolly, K.F. Johnson, D.P. Sandoval, V. Yuan, A transverse phase-space measurement technique for high-brightness, H^- beams, Nucl. Instrum. Methods A 312 (3) (1992) 415–419.
[5] T. Hofmann, K.O. Kruchinin, A. Bosco, S.M. Gibson, F. Roncarolo, G. Boorman, U. Raich, E. Bravin, J.K. Pozimski, A. Letchford, C. Gabor, Demonstration of a laserwire emittance scanner for the CERN LINAC4 H- beam, Phys. Rev. ST Accel. Beams 18 (2015) 1098–4402.
[6] Nufern, 20/130 Passive LMA double clad fiber, 2013. www.nufern.com. [Online] (Accessed 14 October 2016).
[7] T. Hofmann, et al., Design of a laser-based profile monitor for LINAC4 commissioning at 50 MeV and 100 MeV, in: Proceedings of IBIC15, Melbourne, Australia, 2015.
[8] E. Griesmayer, Cividec instrumentation GmbH, (2015) https://www.cividec.at.
[9] U. Raich, F. Roncarolo, T. Hofmann, Beam instrumentation performance during commissioning of CERN's linac4 to 50 MeV and 100 MeV, in: Proceedings of IPAC2016, Busan, South Korea, 2016.

[10] S.M. Gibson, et al., Experimental results of a compact laserwire system for non-invasive H^- beam profile measurements at CERN's LINAC4, in: Proceedings of IBIC16, Barcelona, Spain, 2016.
[11] T. Hofmann, Development of a Laser-based Emittance Monitor for Negative Hydrogen Beams, (Ph.D. thesis), University of Erlangen-Nuremberg, 2017.
[12] T. Hofmann, G.E. Boorman, A. Bosco, E. Bravin, S.M. Gibson, K.O. Kruchinin, U. Raich, F. Roncarolo, Experimental results of the laserwire emittance scanner for LINAC4 at CERN, Nucl. Instrum. Methods A 830 (2016) 526–531.
[13] T. Hofmann, et al., Results from the laserwire emittance scanner and profile monitor at CERN's LINAC4, in: Proceedings of LINAC16, East-Lansing, MI, USA, 2016.